Error Sources in Cold Atom Inertial Sensors

Nikolaos Dedes, Tim Freegarde
School of Physics and Astronomy, University of Southampton
Building 46, University Road, Southampton, SO17 1BJ
UNITED KINGDOM

n.dedes@soton.ac.uk, tim.freegarde@soton.ac.uk

David Harvey
Thales Research Technology and Innovation
350 Longwater Avenue, Reading, RG2 6GF
UNITED KINGDOM

david.harvey@uk.thalesgroup.com

ABSTRACT

Light-pulse atom interferometry exploits the coherent manipulation of atomic matter-waves by means of laser fields for the detection of inertial quantities such as specific forces, angular rates, gravity, and gravity gradients. In this context, cold atom inertial (CAI) sensors based on light-pulse atom interferometry show much promise for the next generation of navigation systems. Low scale-factor and bias instability make this technology valuable for high accuracy applications in which Global Navigation Satellite System signals are absent or corrupted. Despite the high performance demonstrated in laboratory-based experiments, CAI technology is still far from being deployed in real-world navigation applications. Although solutions have been developed to solve some major drawbacks related to limited bandwidth and dynamic range, and to vibrations and decay of the signal-to-noise ratio in dynamic environments, an analysis of the potential errors that can arise in a CAI sensor must be carried out in order to assess their impact on sensor performance. With this objective we present a detailed analysis of some of the error sources that can arise in a CAI sensor exploiting light-pulse atom interferometry. We specifically consider a sensor architecture using a conventional interferometric scheme based on a sequence of three Raman laser pulses that split, redirect, and recombine the atomic wave-packets. We identify and classify at system level some of the principal error sources, outlining the physical mechanisms behind them and, where possible, attempting a quantitative analysis. Moreover, links between system parameters and sensor performance are provided in order to establish possible limiting factors.

1.0   INTRODUCTION

Strapdown inertial navigation systems utilize measurements of specific forces and angular rates to evaluate the attitude, velocity, and position of a vehicle. However, errors in the measurement process are the main cause of navigation state estimation drifts, which necessitates the integration of an external sensor, such as a Global Navigation Satellite System (GNSS) receiver, to aid in the process [1].

Thanks to their outstanding long-term stability, cold atom inertial (CAI) sensors are a promising technology for strategic grade applications in GNSS-denied environments [2]. State-of-the-art accelerometer triads have demonstrated bias instability levels of 60 ng when tracking the magnitude of the gravity vector in laboratory-based experiments [3], carving the path for next-generation inertial navigation systems. Nevertheless, CAI sensor performance deteriorates in dynamic environments mainly because of decreasing in signal-to-noise ratio due to disturbances such as platform vibrations and rotations, external magnetic fields, and relative motion of the platform with respect to the atomic cloud [4]. In this context, it is crucial to identify and

analyse potential error sources in CAI sensors, their dependency on system parameters, and the impact on sensor and navigation performance.

In our analysis we examine CAI sensors based on light-pulse atom interferometry, wherein three laser pulses divide, redirect, and recombine the atomic matter-waves forming a Mach-Zehnder interferometer. After being trapped, a thermal cloud of atoms freely falls under the action of gravity and ballistically expands because of its finite temperature. Each pulse drives a two-photon Raman transition, in which two laser fields in counterpropagating arrangement are tuned so that their frequency difference matches the hyperfine splitting of the atomic ground states [5]. The inertial information is encoded in the form of a phase shift, and it is due to the relative motion of the laser wavefronts with respect to the atom. The sensitive axis of the CAI sensor is determined by the laser field propagation direction. In the case of the same time between pulses and resonant Raman transitions, the interferometer is insensitive to constant velocity along the sensitive axis and measures the acceleration of the laser wavefronts (rigidly attached to the vehicle) with respect to the atom. The acceleration can be induced by specific forces (linear term) parallel to the sensitive axis or by angular rates (Coriolis term) orthogonal to it; however, in a strapdown configuration, spurious terms stemming from time-varying angular rates, rotations of the specific forces, and centrifugal accelerations determine errors that depend on the vehicle dynamics [6].

The sensitivity function formalism, which was first introduced in the context of atomic clocks, has been widely utilized to assess the effect of various factors on CAI sensor performance. This approach provides both time and frequency domain descriptions of an atom interferometer, enabling the estimation of the response of a CAI sensor to time-varying deterministic and stochastic inputs [7]. The great advantage of the sensitivity function approach in comparison to other methods such as Feynman path integral [6] is that it accounts for the effects of the finite duration of the laser pulse and non-resonant Raman transitions [8].

The structure of the paper is organized as follows. In the first part we analyse the CAI sensor from a system perspective, identifying some of the principal error sources that arise in each functional component. We emphasize the physical mechanisms behind the error sources and analyse their impact upon sensor performance in terms of signal-to-noise ratio, bias, and scale-factor. In the second part we use the sensitivity function formalism to build a sensor error model and provide an estimation of the sensor performance in function of the system parameters. Moreover, the error model is used in a reverse mode to retrieve the system constraints needed to fulfil a target performance for a specific sensor configuration.

2.0   ERROR SOURCES IN A CAI SENSOR

In this Section we analyse some of the error sources that arise in a CAI sensor. Starting from the system architecture of the sensor, we identify the error sources associated with each functional component. Moreover, we disclose the physical mechanism behind them, assessing their impact upon sensor performance.

2.1   System Architecture

CAI sensors based on light-pulse atom interferometry exploit the diffraction of the atomic matter-waves by means of laser fields in order to measure inertial effects. In particular we refer to a CAI sensor in which a free-falling thermal cloud of atoms interacts with three Raman laser pulses in a Mach-Zehnder interferometer. Five functional components can be identified as the main building blocks of a CAI sensor:

- Trapping and cooling. Atoms are loaded from a background vapour into a magneto-optic trap (MOT). Ultra-high vacuum pressure levels ($<10^{-9}$ mbar) are required in order to avoid decoherence induced by atomic collisions with the background gas. Atoms are trapped in the zero of a quadrupole magnetic field and slowed by the scattering force of laser light. Once the atomic thermal velocity is sufficiently small, the quadrupole field is switched off and the intensity of the laser

decreased, further reducing the thermal velocity distribution width to an equivalent temperature of few µK [9].

- State preparation. At the end of the trapping and cooling stage, the atomic cloud is released from the MOT, and atoms populate all the Zeeman magnetic sub-levels, m_F, within a hyperfine ground state. By means of optical pumping and micro-wave pulses, atoms are prepared in the $m_F=0$ state, which is insensitive, at first order, to magnetic fields. In some cases, additional laser pulses are used in order to select a fraction of atoms belonging to lower velocity classes.

- Raman pulse sequence. Atoms prepared in the $m_F=0$ state interact with three Raman laser pulses. The first pulse acts like a beam-splitter and diffracts the atomic wave-function in a coherent superposition of two states, $|g, \mathbf{p}>$ and $|e, \mathbf{p}+\hbar\mathbf{k}>$. Here we indicated with $|g>$ and $|e>$, respectively the lower and upper hyperfine ground states, with $|\mathbf{p}>$ the momentum state and with $\hbar\mathbf{k}$ the momentum kick impressed by the laser field onto the atomic wave-function. Here $\mathbf{k}$ is the Raman effective wave-vector, given by the difference of laser wave-vectors. After the first pulse, the atomic wave-function is in coherent superposition of both internal and momentum states and evolves freely for a period T. The second pulse acts like a mirror and inverts the atomic states redirecting them. The wave-packets propagate for a second free-evolution period of duration T and at the end of it, a third pulse recombines them ensuring interference. Figure 1 shows the space-time diagram of the wave-function evolution in a Mach-Zehnder interferometer.

- State detection and imaging. The interferometric signal is obtained in the form of a probability by measuring the fraction of atoms in one of the two Mach-Zehnder states. Laser pulses tuned on optical transitions are used to transfer atoms to excited states, during which photons are emitted. By counting the number of photons with a photodetector, the probability to have the atoms in one of the two states - and thus the interferometric signal - can be determined. The magnitude of the signal is represented by the contrast that plays a crucial role in the signal-to-noise ratio. Two main read-out techniques are used in CAI sensors: cloud-averaging and point source interferometry (PSI). In PSI, the interferometric signal is imaged onto a plane in the form of a spatial probability distribution [10]. In cloud-averaging, the interferometric signal is obtained by averaging the probability distribution all over the atomic cloud, thus requiring scanning of the laser phase to extract inertial information [9].

- Processing and output. The inertial information is embedded in the phase of the interferometric signal. Regardless of the read-out scheme, phase extraction requires discrimination of the rotation-induced phase (gyroscope signal) from the acceleration-induced one (accelerometer signal), solution of phase ambiguity, and optimal estimation in presence of low signal-to-noise ratio.

2.2 Error Sources

In each functional component, various error sources emerge. The identification and classification of the error sources is difficult not only because of the complexity of the system, but also because of the couplings between the different error sources. We summarize some of the error sources that arise in a CAI sensor in Table 1, classifying them according to their origin. Moreover, we briefly describe the physical mechanism behind the most important error sources reported in the aforementioned Table, highlighting the impact on the sensor performance in terms of scale-factor, bias, noise, and contrast.

2.2.1 Spatial Distribution of the Initial Atomic Cloud

At the end of the cooling stage, the atoms are trapped in a cloud characterized by a spatial distribution. We evaluate the effects of the shape of the distribution in terms of width and the offset with respect to the Raman axis. The Raman axis is defined by the effective wave-vector direction, and it is coincident with the centroid of the laser intensity profile.
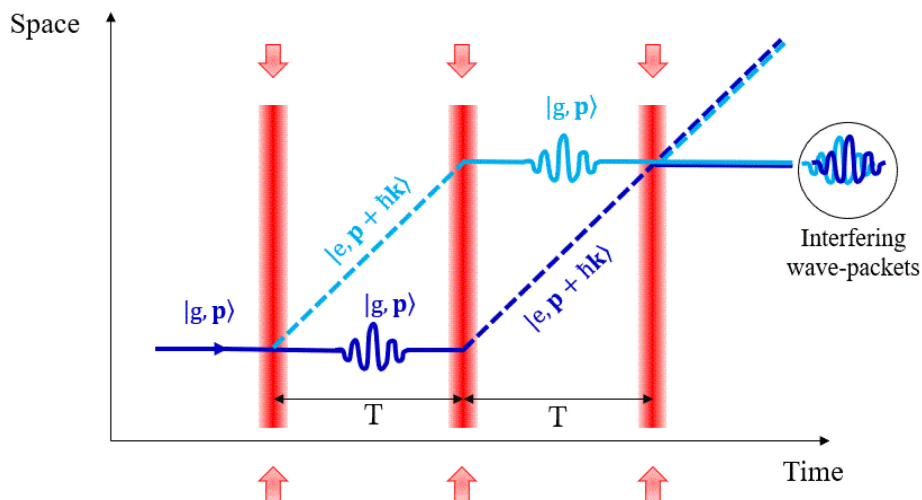
Figure 1: Space-time evolution of the atomic states in a Mach-Zehnder interferometer.

2.2.1.1   *Width of the Distribution*

The contrast of the interferometric signal is influenced by the width of the spatial distribution through three mechanisms. First, couplings with the laser intensity profile affect the efficiency of the Raman transition; for a given velocity distribution, the lower the ratio between the laser waist and the width of the initial spatial distribution, the higher the number of atoms that will experience different laser intensity values, thus reducing the contrast. Second, in a CAI sensor with PSI read-out it couples with angular rates acting in the plane orthogonal to the effective wave-vector direction, reducing the contrast [10]. Indeed, the initial cloud can be thought as an ensemble of point sources that expand in time accumulating a phase shift proportional to the angular rate via the atomic thermal velocity (Coriolis acceleration). When, the cloud is imaged onto a CCD, the averaging process of the phase over the velocity distribution translates into contrast reduction. Third, in a CAI sensor with cloud-averaging read-out, the initial cloud width couples with a time-varying angular rate acting in the plane orthogonal to the effective wave-vector direction, reducing the contrast. This time, each ideal point source carries a phase that depends on the angular acceleration via the atomic initial position (Euler acceleration). Thus, the contrast reduction can be understood as the result of the phase averaging over the space distribution.

In a CAI sensor with PSI read-out, the width of the initial space distribution affects the scale-factor of the gyroscope signal. Physically this is due to the overlap in space of different expanded ideal point sources, each of them carrying an angular rate-dependent phase. The different point sources interfere in such a way the phase shift induced by the angular rate is reduced with respect to the zero-width case [10].

Finally, the width of the initial distribution plays an important role in a variety of bias sources such as wavefront distortions and light-shifts [6], [9]. We address these effects in the related Sections.

Table 1: System component classification of the error sources in a CAI sensor.

Trapping and cooling	• Spatial distribution of the initial atomic cloud. • Atomic velocity distribution in the plane orthogonal to the Raman laser wave-vector. • MOT loading time. • Atomic density.
State preparation	• Atomic velocity distribution in the direction parallel to the Raman laser wave-vector. • Number of atoms in the $m_F \neq 0$ magnetic sublevels.
Raman pulse sequence	• Spatial inhomogeneity of the Raman laser intensity profile. • Collimation of the Raman laser. • Temporal fluctuations of the Raman laser intensity • Light-shifts. • Quadratic Zeeman effect. • Finite duration of the Raman laser pulse. • Raman axis misalignment. • Additional Raman laser frequency components. • Wave-front distortions. • Timing jitter in pulse sequence. • Aliasing due to pulse-mode operation. • Non-linearities in frequency and phase modulation. • Photon spontaneous emissions. • Vehicle dynamics effects. • Gravity gradients.
State detection and imaging	• Atom shot noise. • Photon shot noise. • Frequency and intensity fluctuations of detection laser. • Atomic cloud distortions induced by detection laser. • Stray lights. • Number of pixels. • Pixel-to-pixel sensitivity variations. • Imaging blurring and distortions. • Photodetector technical noise and non-linearities.
Processing and output	• Phase ambiguity. • Impact of signal-to-noise ratio on phase optimal estimation. • Discrimination of the rotation-induced phase from the acceleration-induced one. • Tracking fast-varying signals in dynamic environments.

2.2.1.2   *Offset of the Distribution*

The offset of the initial space distribution with respect to the Raman axis is a measure of its degree of asymmetry. The first effect is related to contrast decay when the laser beam exhibits a spatially varying intensity profile such as in the case of a gaussian beam. Because of the offset, the atoms do not experience the nominal value of intensity, and this decrease the efficiency of the Raman transition.

The second effect is related to phase shift errors. The offset of the distribution couples with wavefront distortions that do not exhibit radial symmetry, hence a bias is induced. A subtle effect is related to the bias that arises in cloud-averaging CAI sensors during the detection when coupled with an angular rate acting in the plane orthogonal to the Raman axis [11]. Because of the intensity profile of the detection laser and the optics involved, the detection process is characterized by a response function. The interferometric signal is obtained as a convolution of the atomic distribution at the end of the Mach-Zehnder sequence with the detection response function. An offset of the cloud with respect to the centre of the response function determines an asymmetric averaging of the velocity distribution and a bias on the accelerometer signal. Finally, the distribution offset induces a bias in presence of angular accelerations or a scale-factor error in the case of non-resonant pulses. The first effect can be understood in terms of Euler acceleration. The second is due to residual sensitivity to initial velocity that arises in an asymmetric Mach-Zehnder pulse sequence: indeed, the centre of mass of the cloud, displaced with respect the Raman axis and subject to an angular rate orthogonal to it, experiences a velocity along the wave-vector direction.

2.2.2   Atomic Velocity Distribution

The atomic cloud entering in the Mach-Zehnder pulse sequence is a thermal ensemble characterized by a 3D velocity distribution. As done for the space distribution, we analyse the effects of the velocity distribution in terms of width and offset. Moreover, we distinguish between the effects of the distribution in the parallel and orthogonal direction to the Raman axis.

2.2.2.1   *Width of the Distribution*

The primary effect of the velocity distribution is related to the contrast of the interferometric signal. The widths of the distribution in the parallel and orthogonal direction to the Raman axis affect the contrast through two different mechanisms. The width in the plane orthogonal to the laser axis determines the expansion rate of the atomic cloud: the higher the width, the more the atoms that will experience different laser intensities and, thus, a decreased efficiency in the Raman diffraction process. The width in the direction of laser propagation axis affects the Raman transition via the Doppler effect: the atomic energy levels are shifted according to the atomic velocity, thus modifying the resonance condition.

Another mechanism through which the width of the velocity distribution in the plane orthogonal to the wave-vector reduces the contrast is when coupled with an angular rate acting in the same plane [4]. The angular rate rotates the laser wavefronts imprinting a time-varying momentum kick to the atomic trajectories that causes a non-perfect overlap of the wave-packets at the third laser pulse. The overlap depends on the physical extension of the wave-packets that is inversely proportional to the velocity width according to the Heisenberg principle.

Finally, the width of the velocity distribution in the transverse direction to the Raman axis affects the bias of a CAI sensor when coupled to wavefront distortions. This effect is addressed in detail in Section 2.1.6.

2.2.2.2   *Offset of the Distribution*

A velocity offset determines a bias on a CAI sensor when coupled to magnetic field and gravity gradients in in the same direction of the Raman axis. An additional bias arises when the interferometric pulse sequence exhibits asymmetries with respect to the central pulse.

In contrast, a velocity offset in the transverse direction to the Raman axis produces, as a primary effect, a phase shift via Coriolis effect. As a result, the accelerometer signal is affected by a bias that depends on the angular rate acting in the same transverse plane.

2.2.3   Space Profile of the Raman Laser Intensity

Raman laser beams with gaussian intensity profiles are usually used in light-pulse atom interferometry applications. Gaussian beams are easy to realize experimentally and allow high peak intensities to be achieved. However, the spatial inhomogeneity of the intensity profile couples with the expansion of the atomic cloud in the plane orthogonal to the wave-vector direction thus inducing a decay in the contrast of the interferometric signal that depends on the width of the atomic space and velocity distributions and on the waist of the intensity profile. In practice the intensity profile differs from a gaussian mode: high order Gauss-Laguerre modes, and localized inhomogeneities, such as bright spots and intensity rings, affect the interferometric signal further reducing the contrast [9].

Moreover, intensity variations have an effect on the wavefront profile causing scale-factor, bias, and noise errors. As an example, a laser beam that has a perfect gaussian intensity profile exhibits two non-linear phase components: a quadratic term characterized by a constant radius of curvature that primarily induces a bias, and another one known as Gouy phase, source of scale-factor errors [12]. The first term is a direct consequence of the fact that a gaussian function is invariant under Fourier transform, thus giving rise to a quadratic position-dependent phase shift. The origin of the Gouy phase can be explained in terms of conservation of momentum. A radial variation of the intensity along the propagation axis determines a variation of the wave-vector in the same direction; as a consequence of momentum conservation, a radial momentum arises [12]. Finally, high spatial intensity noise, due for example to poor quality optics, induces short-scale phase fluctuations that locally modify the wavefront and lead to additional noise [12].

2.2.4   Temporal Fluctuations of the Raman Laser Intensity

Inter-pulse variations of the Raman laser intensity are mainly bias and scale-factor error sources. Asymmetries with respect to the central mirror pulse due to the laser intensity variations experienced by the atomic ensemble introduce sensitivity to initial velocity along the Raman axis [2]. In ideal conditions, the initial velocity-dependent phase accumulated by the atomic wavefunction cancels out because the wave-packets spend equal superposition times in both halves of the interferometer. However, when asymmetries in the pulse sequence occur, the effective superposition time spent by the wave-packets in the two interferometer halves slightly differs, thus causing a bias.

The scale-factor of an atom interferometer is proportional to the area enclosed by the trajectories of the upper and lower states in the Mach-Zehnder sequence [13]. This area is determined by the momentum kick impressed by the laser fields onto the atomic wavefunction. Deviations of the laser intensity from the nominal value induce variations in the atomic trajectories and, hence, scale-factor errors in a CAI sensor.

Atoms experience inter-pulse intensity variations because of low-frequency stochastic fluctuations or relative motion with respect to an inhomogeneous intensity profile. The relative motion is induced by the ballistic expansion of the atomic cloud or by accelerations in the direction orthogonal to the beam propagation axis.

2.2.4.1   Light-Shifts

Stimulated Raman transitions couple states $|g, \mathbf{p}\rangle$ and $|e, \mathbf{p}+\hbar\mathbf{k}\rangle$ via a far-detuned upper state. Light-shifts represent self-coupling terms that shift the atomic energy levels according to the laser intensity, the polarization, and the detuning from the upper state. Light-shifts are usually suppressed by adjusting opportunely laser intensities or frequencies. However, laser intensity variations from the nominal value determine the residual sensitivity to light-shifts. High-frequency laser intensity fluctuations determine noise,

while long-term drifts induce bias. Physically, the noise is determined by intra-pulse intensity fluctuations, while the bias is determined by the asymmetries induced by the expansion of the atomic cloud in presence of spatial intensity inhomogeneities [10].

Additional light-shifts arise when the laser counterpropagating arrangement is realized with a retroreflecting mirror. The presence of both momentum states |e, **p**±ℏ**k**> in the Raman diffraction process allows double transitions in both wave-vector directions. However, in order to realize a single diffraction process, laser frequencies must be tuned on one of the two transitions. The off-resonant transition shifts the energy level of the resonant one proportionally to the laser intensity, thus inducing an additional bias on the CAI sensor [3].

2.2.5   Quadratic Zeeman Effect

The energy levels of atoms in the $m_F=0$ Zeeman state exhibit a quadratic magnetic field dependency. A DC field does not affect a CAI sensor, because the phase accumulated by the atomic wavefunction is the same in the two halves of the interferometer. However, if the atoms experience time-varying magnetic fields during the interferometric sequence a phase error arises. Magnetic fields affect a CAI sensor through three main mechanisms [4]:

- Temporal fluctuations. Purely temporal magnetic field fluctuations are mainly due to eddy currents and residual magnetic noise. Eddy currents manifest as transients of the switch-on/off of the magnetic coils during the trapping stage and are a bias source. Magnetic noise affects the interferometer at time-scales of the order of the free-evolution period and is a noise source for the CAI sensor.

- Spatial variations along the Raman axis. Spatial inhomogeneities of the magnetic field couples with atomic trajectories along the Raman axis giving rise to bias and scale-factor errors.

- Magnetic gradient force. A spatial variation of the magnetic field determines a state-dependent force that modifies the atomic trajectories in a Mach-Zehnder interferometer introducing a further source of bias and scale-factor errors.

2.2.6   Wavefront Distortions

Non-flatness of the Raman laser wavefront represents one of the major bias sources in CAI sensors [6]. It can be induced by intensity inhomogeneity or by imperfections in the optical elements. The phase error impressed by the distorted wavefront onto the atomic wavefunction depends on the position of the atom within the wavefront itself in the plane orthogonal to the laser beam propagation. For these reasons it is a function of different parameters such as the sensor configuration, the ballistic expansion time of the atomic cloud, the width of the transverse atomic velocity distribution, the type of wavefront distortion, the Raman beam waist, the detection beam radius [6], [14]. Long-term drifts in atomic trajectories are a major source of bias instability when coupled with wavefront distortions. Moreover, wavefront distortions are a noise source when coupled with high-frequency trajectory fluctuations induced by vibrations [6].

2.2.7   Aliasing Due to Pulse-Mode Operation

Aliasing noise impacts the performance of CAI sensors that operate in pulse-mode, as dead times associated with the various stages of trapping, cooling, preparation, and atom detection are unavoidable. [7]. During the dead times there is no measurement, resulting in uncorrelated noise from different sensor cycles. This has a direct effect on the slope of the Allan deviation of the interferometric signal, that scales as $\sim 1/\sqrt{\tau}$. The dominant source of aliasing is due to vibrations which displace the laser wavefronts, thus impressing random phases onto the atomic wavefunction. Laser phase noise represents another source of aliasing. Vibrations mainly affect the CAI sensor at time-scales of the order of the interferometer duration, while phase noise manifests at time-scales of the order of the pulse duration.

2.2.8 Vehicle Dynamics Effects

The effect of the vehicle dynamics manifests in different ways. Angular rates and accelerations in the direction orthogonal to the Raman axis induce decay of contrast as described in the previous Sections. Accelerations in the Raman axis direction cause a further decay in signal-to-noise ratio via the Doppler effect.

A further impact is represented by high-order inertial effects due to couplings between accelerations and angular rates acting along axis orthogonal to the sensitive one. This error source is analogous to anisoinertia bias in classic inertial sensors and manifests as the result of the rotation of the laser wavefronts with respect to a reference frame. The bias strongly depends on the level of the acceleration and angular rate and on the free-evolution period T.

2.2.9 Atom Shot Noise

Atom shot noise sets the ultimate theoretical limit of a CAI sensor operating with unentangled atoms and its nature is purely statistical [9]. At the end of the Raman pulse sequence, the Mach-Zehnder interferometer presents two output ports in which the probability to find the atoms in one of the two states follows, in the approximation of central limit theorem, a gaussian distribution with standard deviation $1/\sqrt{N}$, where N is the total number of detected atoms.

3.0 CAI SENSOR ERROR MODEL

In this Section, we use the sensitivity function formalism to quantitatively estimate the impact of several error sources upon the performance of a cold atom accelerometer. The impulsive response function (IRF), $h_\xi(t)$, describes the phase response of the interferometer, $\Delta\varphi$, to a time-varying input, $\xi(t)$,

$$\Delta\varphi = \int h_\xi(t)\, \xi(t)\, dt \,, \tag{1}$$

where the integral is computed over the cycling period of the sensor. In the frequency domain, the sensitivity function allows the estimation of the sensor uncertainty in terms of Allan variance. In the hypothesis of error sources characterized by a constant power spectral density, S_ξ (white noise), and cluster time τ much higher than the sensor cycling period, T_C, the Allan variance of the interferometric phase is [7]

$$AVAR_{\Delta\varphi} = (S_\xi / \tau) \sum_n |H_n|^2, \tag{2}$$

with H_n, Fourier transform of the IRF evaluated at the n-th multiple integer of the cycling frequency. In Equation (2) the sum is computed for all n. The Allan variance of the accelerometer signal is obtained dividing the phase Allan variance by the accelerometer scale-factor.

As a proof of principle of the potential of the method, we compute the phase shift and the phase Allan variance induced by a selected group of error sources. We assume flat wavefronts and, when possible, that the duration of each laser pulse is much shorter than the free-evolution time.

3.1 Temporal Fluctuations of the Raman Laser Intensity

Assuming a temporal intensity fluctuation, δI, with respect to the nominal values, I_1 and I_2, a bias phase arises on the interferometer signal as the result of asymmetries induced by the expansion of the atomic cloud into an inhomogeneous intensity profile via the light-shift effect. We analytically compute the bias phase considering the evolution of a gaussian atomic phase-space distribution into a gaussian laser beam and infinitesimal pulses

$$\Delta\varphi = K_{LS} (2\tau_P/\pi) (1-r) [1/(1+4\sigma_3^2/w^2) - 1/(1+4\sigma_1^2/w^2)] \,\delta I \,, \tag{3}$$

where K_{LS} is the light-shift coupling constant that depends on the laser polarization, on the detuning from the excited transition and on the nominal laser intensity, $r=I_1/I_2$ is the ratio between the nominal intensities of the two Raman laser fields, τ_P is the duration of the beam-splitter pulse, w is the Raman beam waist, and σ_i is the standard deviation of the atomic space distribution at the i-th pulse. Equation 3 highlights an intuitive result: the bias phase shift induced by the light-shift strongly depends on the ratio between the size of the atomic cloud and the Raman beam. Indeed, the larger the cloud expansion, the higher the degree of asymmetry that the atoms experience during the Raman pulse sequence and, thus, the higher the bias phase.

The interferometric phase shift subject to a steady specific force defines the scale-factor of the accelerometer signal:

$$\Delta\varphi = \mathbf{k^b} \cdot \mathbf{f_{ib}^b}T^2 \left[1 + (2+4/\pi)\,\eta + (1+2/\pi)\,\eta\,\delta I/I_j + o(\eta^2)\right], \tag{4}$$

with $\eta = \tau_P/T$ the ratio between the beam-splitter pulse duration and the free-evolution time, I_j the nominal intensity of the j-th laser, $\mathbf{k^b}$ the laser effective wave-vector and $\mathbf{f_{ib}^b}$ the specific force. Note that the phase shift of the CAI sensor exhibits a scale-factor error that depends on the finite pulse duration and on the laser intensity fluctuations. In particular, stochastic fluctuations of the laser intensity determine scale-factor instability.

High-frequency laser intensity fluctuations determine noise on the interferometric signal via the light-shift effect

$$\text{AVAR}_{\Delta\varphi} = (K_{LS}\,I_j)^2 (T_C/\tau)\,S_I\,\tau_P, \tag{5}$$

where T_C is the sensor cycling period, and S_I is the relative intensity noise of the j-th laser field. The physical rationale behind the dependency of the phase Allan variance on pulse duration lies in the fact that the longer the laser is on, the higher the phase noise imparted onto the atomic wavefunction via intensity fluctuations.

3.2   Magnetic Field Effect

Assuming a linear magnetic field gradient, $\partial_z B$, along the Raman axis (z-axis) and infinitesimal pulses, the bias phase shift can be computed as

$$\Delta\varphi = 4\pi K_{QZ}B_0\,\partial_z B\,\left[z_0(\tan(\theta_3/2)/\Omega_3 - \tan(\theta_1/2)/\Omega_1) + (v_{z0}+v_r/2)T^2 + f_z T^3\right], \tag{6}$$

where K_{QZ} is the quadratic Zeeman effect coupling constant and depends on the atomic species, B_0 is a non-zero bias field necessary to define the atomic quantization axis, Ω_i is the Rabi frequency at the i-th pulse and depends essentially on the laser intensity, and $\theta_i = \Omega_i\tau_P$ defines the pulse area that in resonant conditions is equal to $\pi/2$. We note two bias components. The first term depends on the initial position of the atomic cloud along the Raman axis is non-zero only if there is a laser intensity imbalance between the first and last pulse. The second term depends on the initial atomic velocity and on the recoil velocity (i.e., velocity due to the momentum kick imprinted by the laser field to the atom). The scale-factor error exhibits a dependency on T^3. Hence, slow drifts of the value of the bias magnetic field determine both bias and scale-factor instabilities. Drifts in the initial velocity along the Raman axis due, for example, to imbalance in the MOT vertical lasers, are a further source of bias instability.

Small temporal fluctuations with respect to an average magnetic field value determine noise on the interferometric signal given by

$$\text{AVAR}_{\Delta\varphi} = (4\pi K_{QZ}B_0)^2 (T_C/\tau)\,S_B\,T, \tag{7}$$

where S_B is the power spectral density of the magnetic noise. While Equation 7 shares a similar structure with Equation 5, it differs in that the phase noise is predominantly imprinted onto the atomic wavefunction during its free-evolution.

3.4 Pointing Jitter

Fluctuations in the Raman axis direction determines noise on CAI signal given by

$$\mathrm{AVAR}_{\Delta\varphi} = S_\Psi\, (T_C/\tau)\, [\, | \mathbf{k}^b \times \mathbf{L}^b |^2 (\pi^2/4\tau_P) + | \mathbf{k}^b \times \mathbf{v}^b |^2 (3\pi^2 T^2/8\tau_P) + (\mathbf{k}^b \times \mathbf{L}^b)\cdot(\mathbf{k}^b \times \mathbf{v}^b)(\pi^2 T/2\tau_P)\,]\,, \qquad (8)$$

where S_Ψ is the white noise power spectral density of the pointing jitter expressed in rad^2/Hz, $\mathbf{v}^b$ is the mean atomic velocity and $\mathbf{L}^b$ is the offset of the atomic space distribution with respect to the Raman axis. We note that the noise depends on both the position and velocity offset of the atomic cloud in the transverse direction to the Raman axis.

3.5 Performance Analysis

In Figure 2 we show an example of performance analysis calculation for a cold atom accelerometer. For our analysis we consider a cloud of ^{85}Rb atoms with a velocity distribution corresponding to an effective temperature of 10μK. Raman laser beams with gaussian intensity profiles characterized by a 7mm waist and nominal powers of 63.7mW and 95.55mW have been assumed. The two laser fields are orthogonally polarized in a σ^+/σ^+ configuration with single photon detuning Δ=5GHz. This configuration is equivalent to a pulse duration τ_P~20μs. We analyse the impact of slow laser intensity drifts on scale-factor and bias instabilities via Equations (3) and (4) for different τ_P/T. The plot shows that even for relative intensity drift of 1%, $\tau_P/T < 0.04\%$ is needed to realise scale-factor instability below 10 ppm. Bias instability is at most of the order of tenths of nano-g corresponding to a maximum Schuler position error of ~13cm.

Moreover, we quantify the effect of several noise sources upon the short-term sensitivity of the sensor varying the free-evolution time T. For the analysis we assume a unitary contrast. The impacts of pointing jitter of the Raman axis, relative intensity noise, and magnetic field noise have been estimated via Equations (5), (7), and (8). We assume a 0.5mm offset of the atomic cloud with respect to the Raman axis, a mean value of the velocity distribution of 1mm/s in the direction orthogonal to the effective wave-vector, and a bias magnetic field of 50mG applied along the Raman axis. Finally, we assume that the sensor operates at a sampling frequency given by T_S=2T+T_D, with T_D dead time equal to 20ms that accounts for trapping, cooling, state preparation and detection of the interferometric signal. The general trend indicates an enhanced short-term sensitivity for increasing values of the free-evolution time. Physically, this is due to the fact that the cold atom accelerometer behaves like a low-pass filter with a cut-off frequency proportional to 1/T [7]. Hence, the higher the free-evolution time, the lower the sensor bandwidth and the more the high-frequency noise sources are filtered out. Assuming a free-evolution time of T=10ms, in order to realise performance at the 1μg/Hz$^{0.5}$ level, a relative intensity noise below -80 dBc/Hz, a pointing stability higher than the 30nrad/Hz$^{0.5}$ level, and a magnetic noise below 1mG/Hz$^{0.5}$ are required.

4.0 CONCLUSIONS

Light-pulse atom interferometry represents a promising technology for the realization of the next-generation inertial navigation systems. We have identified at system level some of the error source that arise in a CAI sensor characterized by a three-pulse sequence. We have analysed the physical mechanism of each error source high-lighting possible couplings and their impact upon sensor performance. Finally, we have developed a sensor error model based on the sensitivity function formalism in order to evaluate the dependency of sensor performance on system parameters. Under several assumptions, the sensitivity function formalism allows one to obtain analytic expressions, thus providing a tool for a fast estimation of the sensor performance. A more refined error model would involve time-consuming Monte-Carlo simulations in which the evolution of an atomic ensemble is considered.
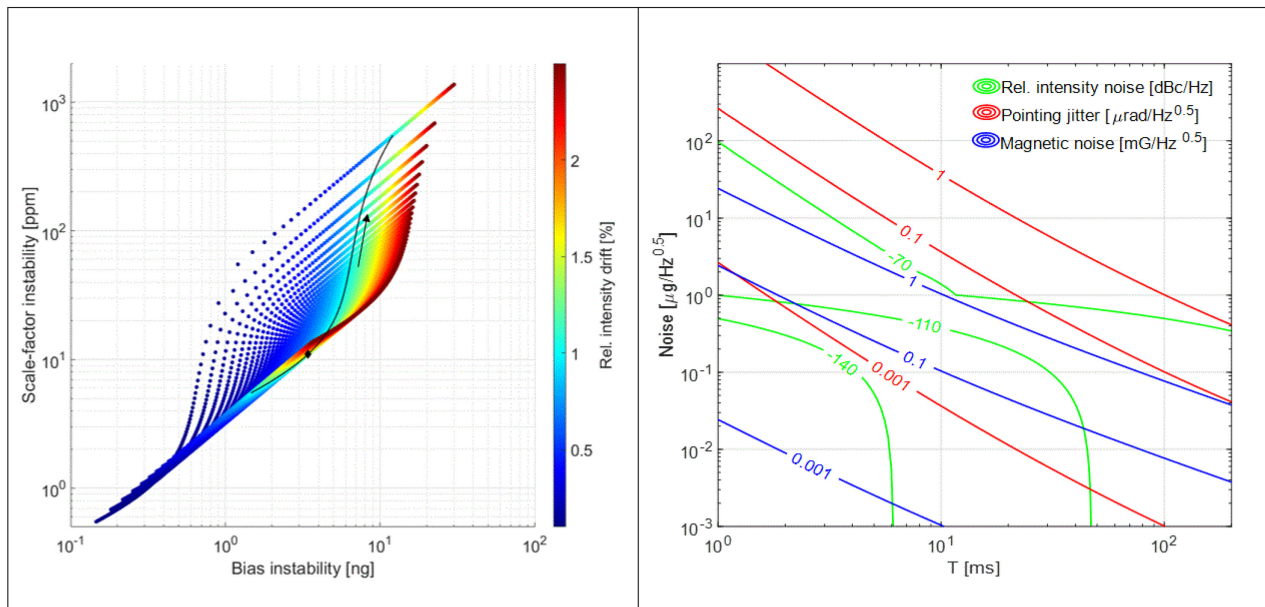
Figure 2: Performance of a cold atom accelerometer. Left panel: Raman relative intensity drift impact on long-term stability performance for different τ_P/T values. The 1% relative intensity isoline is reported in black. The black arrow shows the direction of increasing τ_P/T values. The black diamond indicates the point correspondent to $\tau_P/T = 0.04\%$. Right panel: Impact of relative intensity noise, pointing jitter, and magnetic noise on the accelerometer short-term sensitivity for different T values. The different lines represent loci at constant noise source level.

5.0 ACKNOWLEDGEMENT

6.0 REFERENCES

[1]   Barbour, N., Inertial navigation sensors, Charles Stark Draper Lab Inc. Cambridge MA, USA, Tech. Rep., 2010.

[2]   Yao, Z.W., Chen, H.H., Lu, S.B., Li, R.B., Lu, Z.X., Chen, X.L, Yu, G.H., Jiang, M., Sun, C., Ni, W.T., Wang, J., Zhan, M.S., *Self-alignment of a large-area dual-atom-interferometer gyroscope using parameter-decoupled phase-seeking calibrations*, Phys. Rev. A 103, 023319, 2021.

[3]   Templier, S., Cheiney, P., d' Armagnac de Castanet, Q., Gouraud, B., Porte, H., Napolitano, F., Bouyer, P., Battelier, B., Barrett, B., *Tracking the Vector Acceleration with a Hybrid Quantum Accelerometer Triad*, Sci. Adv., 8 45, eadd3854, 2022.

[4]   Barrett, B., Antoni-Micollier, L., Chichet, L., Battelier, B., Lévèque, T., Landragin A., Bouyer, P., *Dual matter-wave inertial sensors in weightlessness*, Nat. Commun. 7, 13786, 2016.

[5]   Moler, K., Weiss, D., Kasevich, M., Chu, S., *Theoretical analysis of velocity-selective Raman transitions*, Phys. Rev. A 45, 342, 1992.

[6]   Hogan, J., Johnson, D.., Dickerson, S., Kovachy, T., Sugarbaker, A., Chiow, S., Graham, P., Kasevich, M., Saif, B., Rajendran, S., Bouyer, P., Seery, B., Feinberg, L., Keski-Kuha, R., *An atomic gravitational wave interferometric sensor in low earth orbit (AGIS-LEO),* Gen. Relativ. Gravit. 43, 1953–2009, 2011.

[7]   Cheinet, P., Canuel, B., Pereira Dos Santos, F., Gauguet, A., Yver-Leduc, F., Landragin, A., *Measurement of the Sensitivity Function in a Time-Domain Atomic Interferometer*, IEEE Trans. Instrum. Meas., vol. 57, no. 6, pp. 1141-1148, 2008.

[8]   Bonnin, A., Zahzam, N., Bidel, Y., Bresson, A., *Characterization of a simultaneous dual-species atom interferometer for a quantum test of the weak equivalence principle*, Phys. Rev. A 92, 023626, 2015.

[9]   Peters, A., Chung, K., Chu, S., *High-precision gravity measurements using atom interferometry*, Metrologia 38 25, 2001.

[10]   Hoth, G., Pelle, B., Riedl, S., Kitching, J., Donley, E., *Point source atom interferometry with a cloud of finite size*, Appl. Phys. Lett. 109, 071113, 2016.

[11]   Farah, T., Gillot, P., Cheng, B., Landragin, A., Merlet, S., Pereira Dos Santos, F., *Effective velocity distribution in an atom gravimeter: Effect of the convolution with the response of the detection*, Phys. Rev. A 90, 023606, 2014.

[12]   Bade, S., Djadaojee, L., Andia, M., Clade, P., Guellati-Khelifa, S., Observation of Extra Photon Recoil in a Distorted Optical Field, Phys. Rev. Lett. 121, 073603, 2018.

[13]   Antoine, C., *Rotating matter-wave beam splitters and consequences for atom gyrometers*, Phys. Rev. A 76, 033609, 2007.

[14]   Schkolnik, V., Leykauf, B., Hauth, M., Freier, C., Peters, A., *The effect of wavefront aberrations in atom interferometry*, Appl. Phys. B 120, 311–316, 2015.